Supplementary Information

Correlating microscopic viscoelasticity and structure of an aging colloidal gel using active microrheology and cryogenic scanning electron microscopy

Rajkumar Biswas[1, †], Vaibhav Raj Singh Parmar[1, ‡], Anson G Thambi[1, ‡], and Ranjini Bandyopadhyay[1,*]

[1] *Soft Condensed Matter Group, Raman Research Institute, C. V. Raman Avenue, Sadashivanagar, Bangalore 560 080, INDIA*

February 20, 2023

[†] rajkumar@rri.res.in
[‡] vaibhav@rri.res.in
[§] anson@rrimail.rri.res.in
[*] Corresponding Author: Ranjini Bandyopadhyay; Email: ranjini@rri.res.in

ST1 Schematic diagram of microchannel used in OT experiments

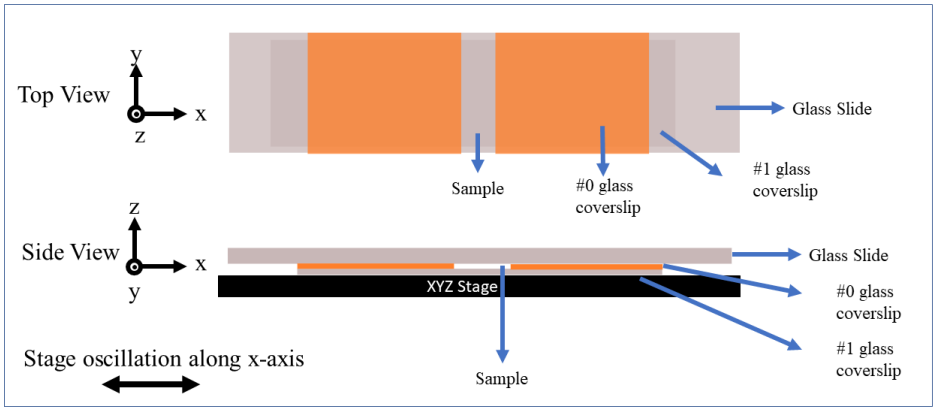

Supplementary Fig. S1: Schematic illustration of the glass microchannel used for the OT experiments. Active microrheology measurements are performed by oscillating the XYZ stage along the x axis.

ST2 Piezoelectric stage calibration: calculation of the voltage-displacement conversion factor for controlled movement of the sample stage

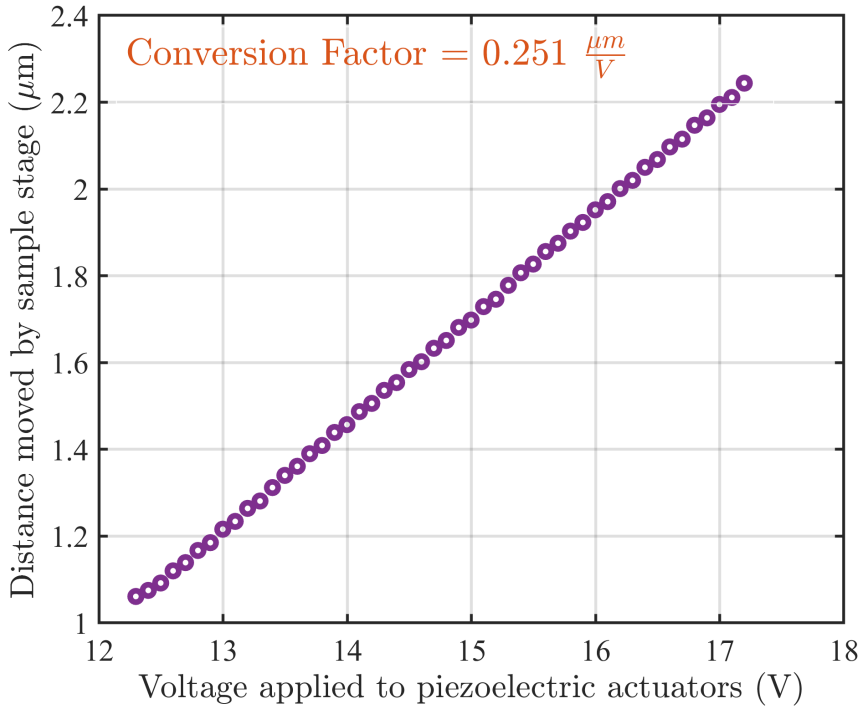

Supplementary Fig. S2: Distance traveled by the sample stage is measured as a function of the voltage applied to the piezo actuator. The calibration factor, computed from the slope of the curve, is 0.251 μm/V.

The sample stage consists of a slide holder with a 3-axis XYZ translational stage, piezoelectric actuators and strain gauges. Application of a voltage to the piezoelectric actuators results in the desired oscillation of the sample stage. The strain gauges measure the accurate position of the sample stage feedback for controlled spatial movement.

The conversion factor for calibrating the voltage applied to the piezoelectric actuators to the net distance travelled by the sample stage is next computed. We prepare a glass microchannel containing a tiny amount of polystyrene beads suspended in 0.5 mM NaCl aqueous solution. The beads get attached to the glass coverslip in a high salt environment which allows us to acquire the bead position using a CMOS camera as we apply a voltage to the piezoelectric actuators. The slope of the plot of stage displacement versus voltage applied to the piezoelectric actuators gives a voltage to displacement

conversion factor of 0.251 μm/V (Supplementary Fig. S2).

ST3 Quadrant photodiode (QPD) position calibration

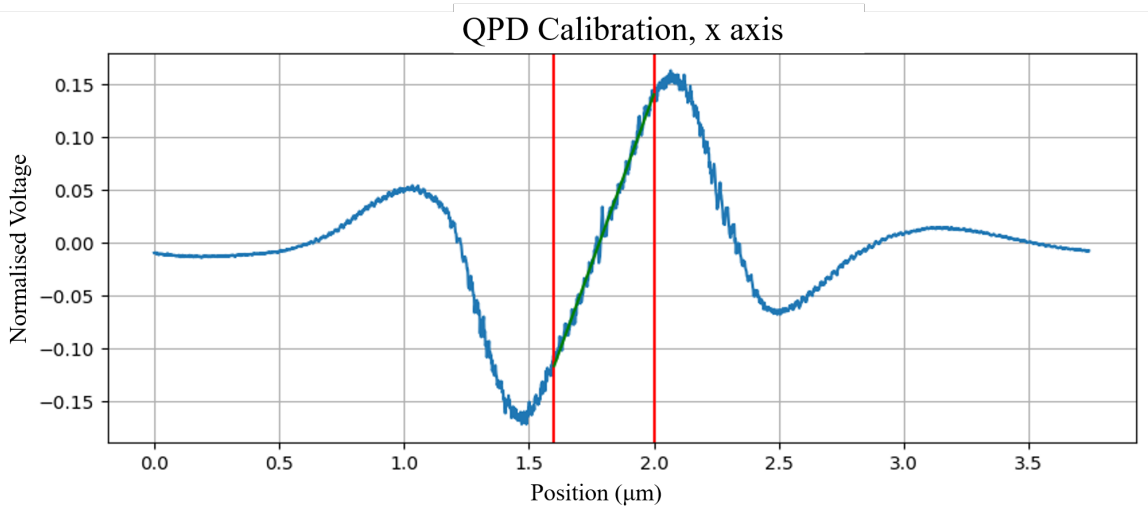

Supplementary Fig. S3: Position calibration of QPD is performed by shifting a bead attached to a glass coverslip along the x-axis by a predetermined distance from the laser's beam center. The QPD signal is acquired during this movement and plotted against the motion of the trapped bead. We determine the sensitivity of the QPD, 1.51 nm/QPD unit, by fitting the linear region of the curve with a straight line.

High-frequency position measurement of an optically trapped bead using a quadrant photodiode requires a relation between QPD output voltage and bead position data. To determine this relation, also called QPD sensitivity, we moved a bead attached to the glass coverslip along the x and y axes such that the bead passes through the center of the laser spot while QPD output voltages are simultaneosuly measured. The QPD output voltage is linearly related to the bead position in a narrow trap region between the two parallel red lines as displayed in Supplementary Fig. S3. The slope of the linear region yields a QPD sensitivity of 1.51 nm/QPD unit.

ST4 Measurement of trap stiffness using power spectrum method

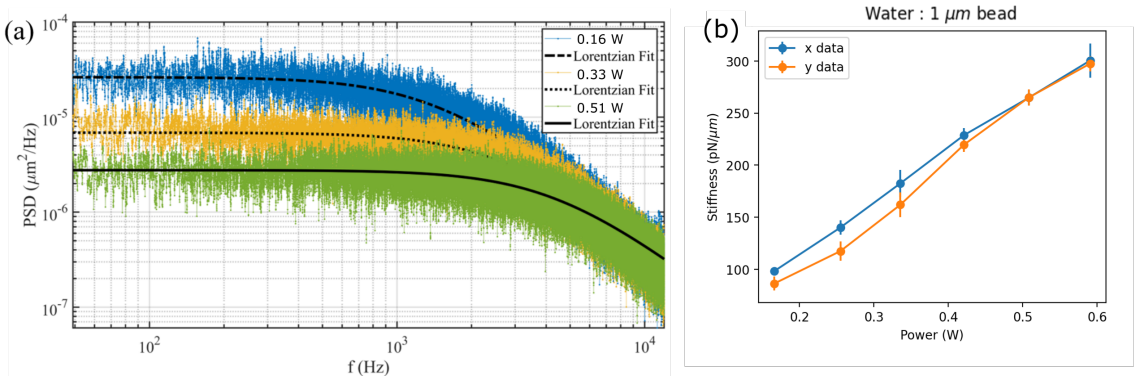

Supplementary Fig. S4: (a) Power spectral density (PSD) is plotted for three values of incident laser power and fitted with Lorentzian functions to determine the trap stiffness. (b) Trap stiffness is plotted as a function of laser power for displacements along x and y directions.

The trap stiffness depends on incident laser power [1]. We trap a polystyrene bead (1 μm) suspended in water and measure its movement at a sampling frequency of 50 KHz. The Fourier transform of the bead position as shown in Supplementary Fig. S4(a) is fitted to the Lorentzian function, $PSD = A/(f^2+{f_c}^2)$, where A depends on the surrounding temperature, f is the frequency, $f_c = \kappa/2\pi\gamma$ is the corner frequency and γ is the coefficient of the viscosity of the medium [1]. The trap stiffness κ increases with laser power as shown in Supplementary Fig. S4(b).

ST5 Cryo-FESEM

Cryo-FESEM images of PS particles of different sizes attached to Laponite networks.

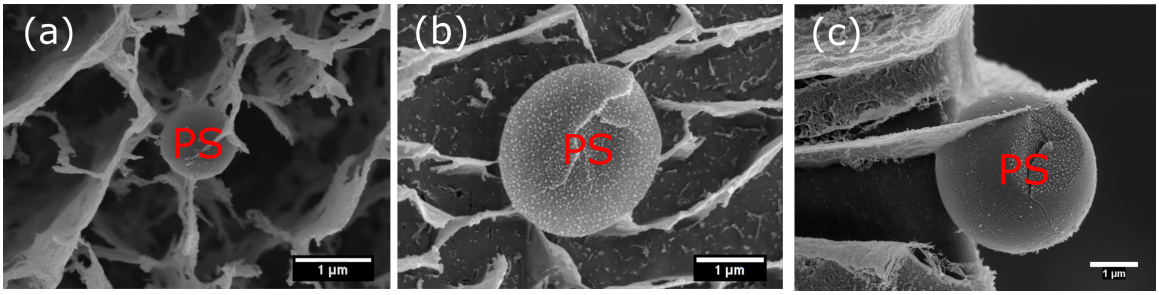

Supplementary Fig. S5: Polystyrene (PS) particles attached to the branches of the Laponite suspension networks (white connected regions) for particles of diameter (a) 1 μm (b) 1.5 μm and (c) 3.34 μm.

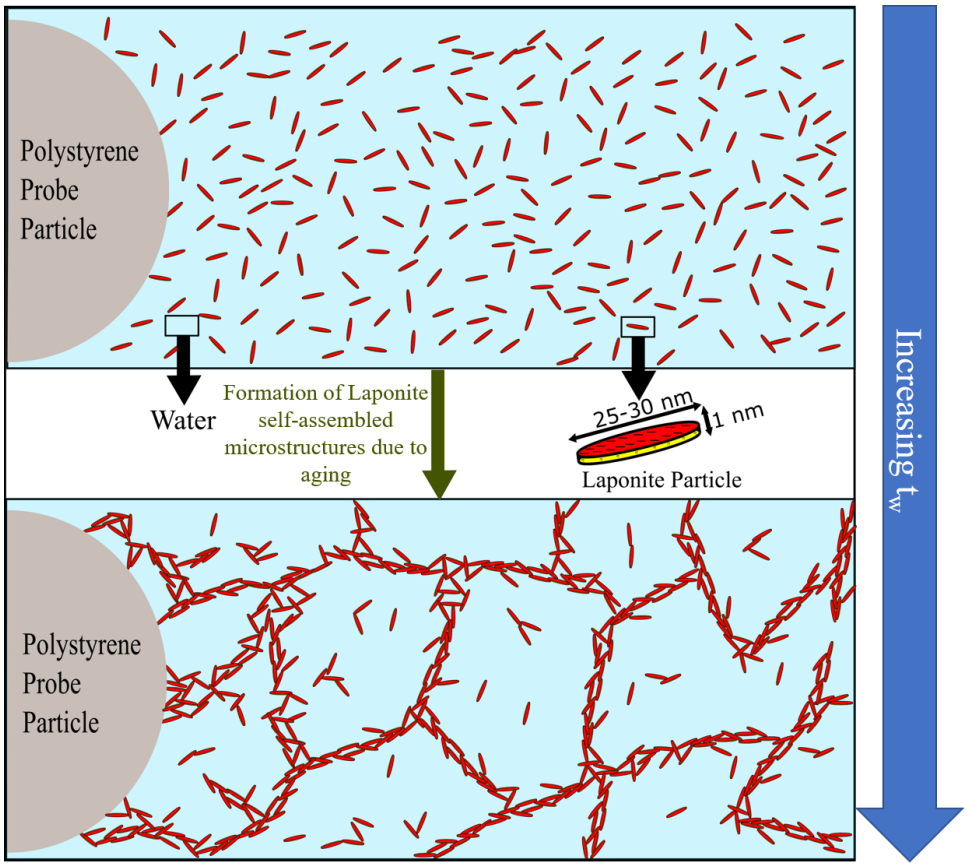

Supplementary Fig. S6: Schematic illustration showing the temporal evolution of Laponite microstructure in the presence of a polystyrene probe particle. Top panel: The probe particle attaches to the Laponite microstructure, with the number of contacts depending on particle size. Bottom panel: Individual Laponite particles self-assemble at higher aging times to form network structures through house of cards and overlapping coin assemblies.

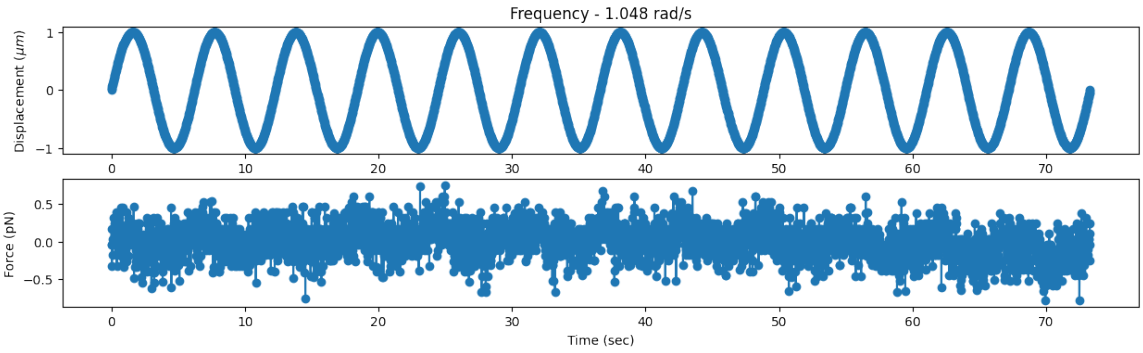

Supplementary Fig. S7: Top: Low frequency (= 1.048 rad/sec) stage oscillation of amplitude 1 μm and Bottom: the corresponding force experienced by the trapped bead of diameter 1 μm. The resultant force is not oscillatory and cannot be analyzed to determine the mechanical properties of the Laponite suspension at this frequency.

ST6 Error calculation

For each measurement, 12 sinusoidal oscillations have been implemented and the force on the trapped bead has been measured. We have excluded the initial and the final oscillations to avoid any artefact driven by transient signals. To compute error bars in measuring G' and G'', we have therefore used the ten intermediate oscillations. The computed values of G' and G'' are seen to be reasonably consistent and the deviations for these ten different cycles are presented as error bars.

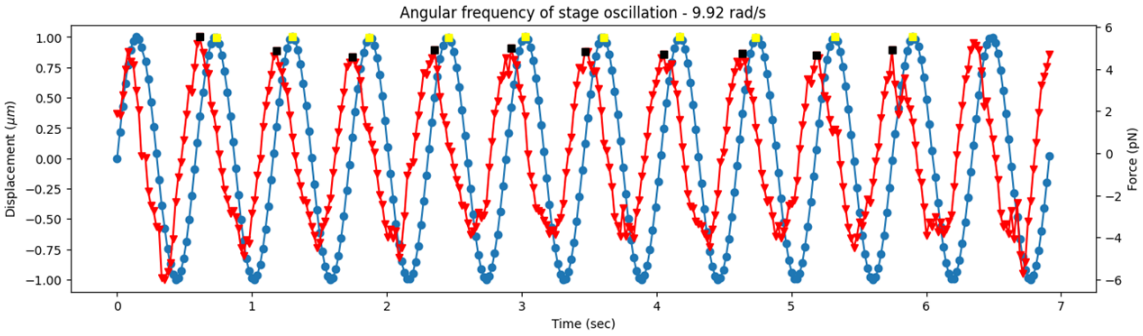

Supplementary Fig. S8: The blue curve with solid circles indicates the stage position with time. The peaks in the signal are detected using scipy module in Python. The peaks in the stage oscillation signals are indicated using yellow squares. The force on the trapped particle is shown by the red curve with red triangles. The black squares indicate the peaks of the force signal.

Ten peaks, after excluding the first and last oscillations, are used to calculate the time difference between the peaks of the applied stage displacement and the corresponding force measurement (Supplementary Fig.S8). This results in 10 estimates of time differences which are used to compute the mean and standard deviation in the measured phase angle using the protocol below,

$$t_{diff} = mean(t_1, t_2, \ldots., t_{10})$$

$$t_{error} = standard\, deviation(t_1, t_2, \ldots., t_{10})$$

Phase angles in degree are estimated computing,

$$\phi_{diff} = 360^{\circ} * f * t_{diff},\ \phi_{error} = 360^{\circ} * f * t_{error}$$

where f = stage oscillation frequency (in Hz)

The mean and standard deviation of the phase angles calculated according to the method as described above are used to calculate the mean and standard deviation values of the elastic and viscous moduli using the relations (Eqns. 1 and 2 of the manuscript),

$$G' = \frac{F_{max}}{6\pi R X_{max}} cos(\frac{\pi\phi_{diff}}{180}),\ \Delta G' = \frac{F_{max}}{6\pi R X_{max}} sin(\frac{\pi\phi_{diff}}{180})(\pi\phi_{error}/180)$$

$$G'' = \frac{F_{max}}{6\pi R X_{max}} sin(\frac{\pi\phi_{diff}}{180}),\ \Delta G'' = \frac{F_{max}}{6\pi R X_{max}} cos(\frac{\pi\phi_{diff}}{180})(\pi\phi_{error}/180)$$

where $\Delta\phi = \frac{\pi\phi_{diff}}{180}$.

G' and G'' with error bars are plotted in transparent colors in the Supplementary Fig. S9. The maximum error propagation while computing G_{co} and ω_{co} is estimated by considering the maximum ranges of errors of these two variables, marked using the dashed lines for both horizontal and vertical directions. To calculate the errors in crossover modulus G_{co} and relaxation time τ_{co}, the following relations have been used:

$$G_{co} = (G_{co2} + G_{co1})/2,\ \Delta G_{co} = (G_{co2} - G_{co1})/2$$

$$\omega_{co} = (\omega_{co2} + \omega_{co1})/2,\ \Delta\omega_{co} = (\omega_{co2} - \omega_{co1})/2$$

$$\tau_{co} = 2\pi/\omega_{co},\ \Delta\tau_{co} = (2\pi/\omega_{co}^2)\Delta\omega_{co}$$

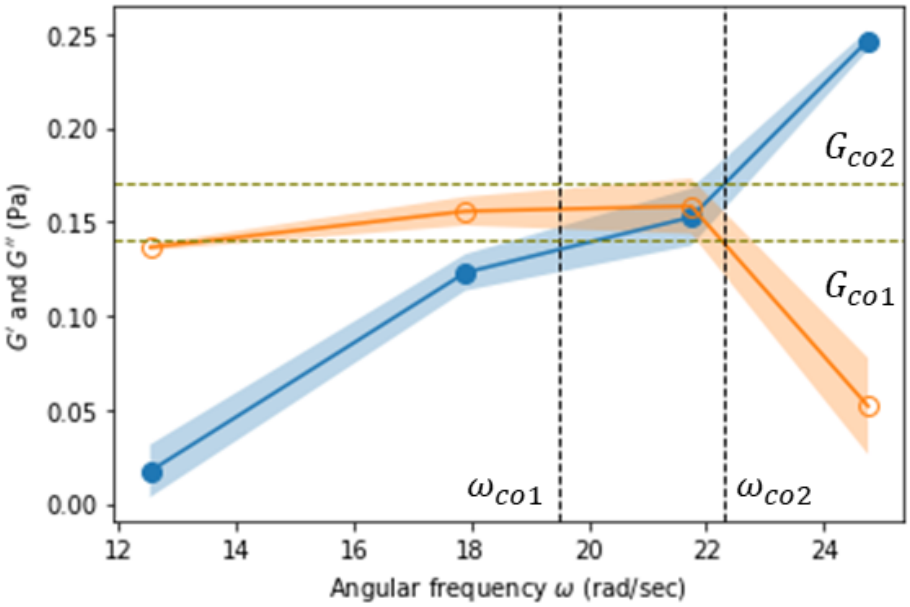

Supplementary Fig. S9: G' (solid blue symbols) and G'' (hollow orange symbols) and the corresponding error bars are shown by the shaded regions of the same colour. The maximum possible ranges of the crossover values of the moduli and angular frequencies are marked using the dashed horizontal and vertical lines.

ST7 Bulk rheology measurement of Laponite suspension

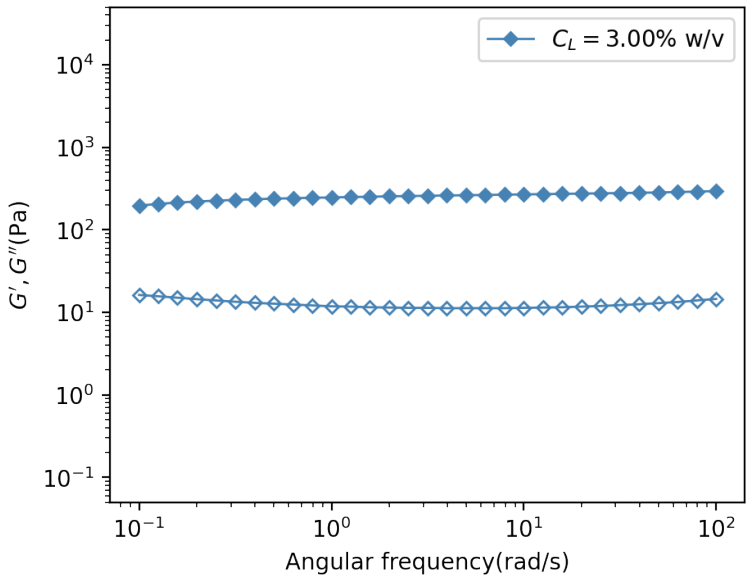

Supplementary Fig. S10: Macroscopic or bulk elastic (G', solid symbols) and viscous (G'', hollow symbols) moduli of a Laponite suspension of concentration $C_L = 3.00\%$ w/v at aging time $t_W = 90$ min as measured using a rheometer.

ST8 Active microrheology measurements using 1 μm probe particle for Laponite suspensions of concentration C_L = 2.75% w/v at various aging times t_w

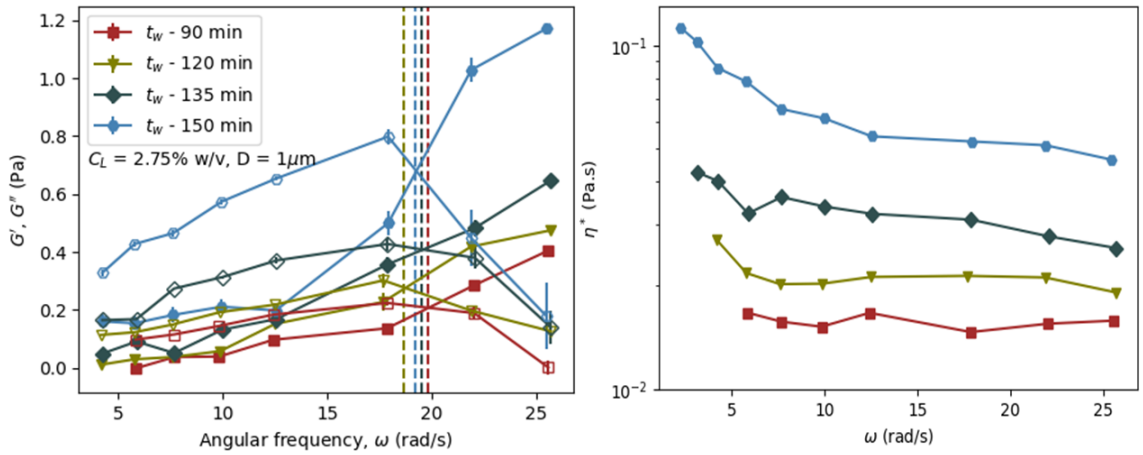

Supplementary Fig. S11: (a) Elastic and viscous moduli, G′ (solid symbols) and G″ (hollow symbols) respectively, are estimated using oscillatory active microrheology for a 2.75% w/v Laponite suspension at different aging times t_w. (b) The values of complex viscosity η^*, estimated using $\eta^* = \sqrt{(G'^2 + G''^2)}/\omega$, are plotted *vs.* angular frequency, ω, for suspensions of the same aging times as in (a).

ST9 Active microrheology measurements for 2.5% w/v Laponite suspensions at aging time t_w = 90 minutes using probe particles of different sizes D

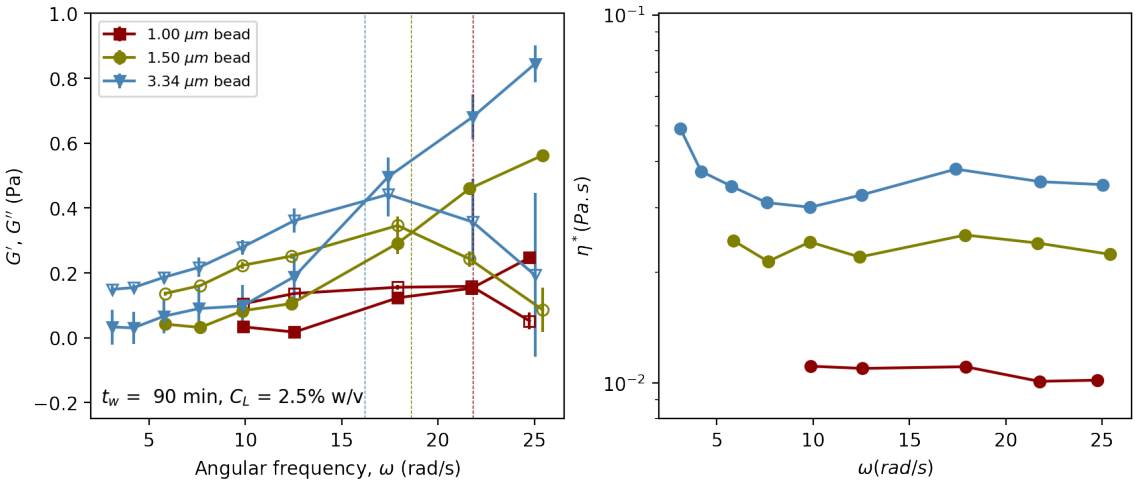

Supplementary Fig. S12: (a) G′ (solid symbols) and G″ (hollow symbols) are estimated for a 2.5% w/v Laponite suspension at aging time t_w = 90 minutes using oscillatory active microrheology with probe particles of different sizes D. (b) The values of complex viscosity η^* are plotted *vs.* angular frequency, ω, obtained by analyzing the same experiments.

ST10 Pore size estimation from cryo-FESEM images

The acquired cryo-FESEM images (a representative image is displayed in Fig. S13 (a)) are initially binarized (binary image is displayed in Fig. S13(b)) to emphasise the Laponite networks using an inbuilt module in the ImageJ software. The area within each pore is measured using ImageJ. The equivalent pore diameter is then estimated by assuming that the measured pore is circular. The average diameter $< D_p >$ is determined by averaging the diameters of various pores (between $\approx$ 10-50). A dimensionless characteristic lengthscale $< D_p/D >$ is estimated by dividing by the probe particle size. The cryo-FESEM image and the corresponding binary image are shown below in Fig. S13.

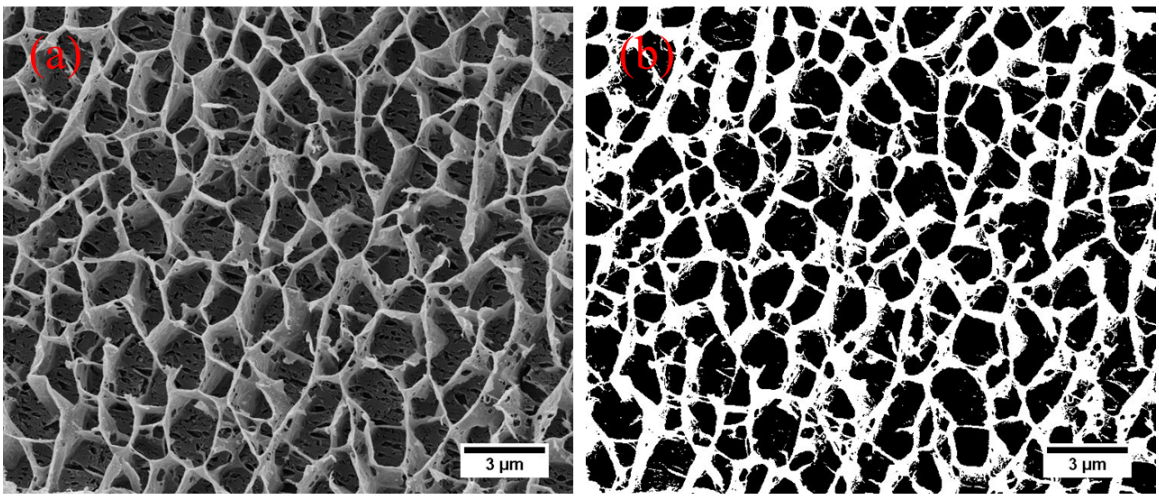

Supplementary Fig. S13: (a) Cryo-FESEM image of Laponite networks of concentration 2.75% w/v at 90 min of aging time after converting to gray-scale. (b) Binarized version of image in (a) used to detect network boundaries.

ST11 Correlation between microstructure and relaxation time

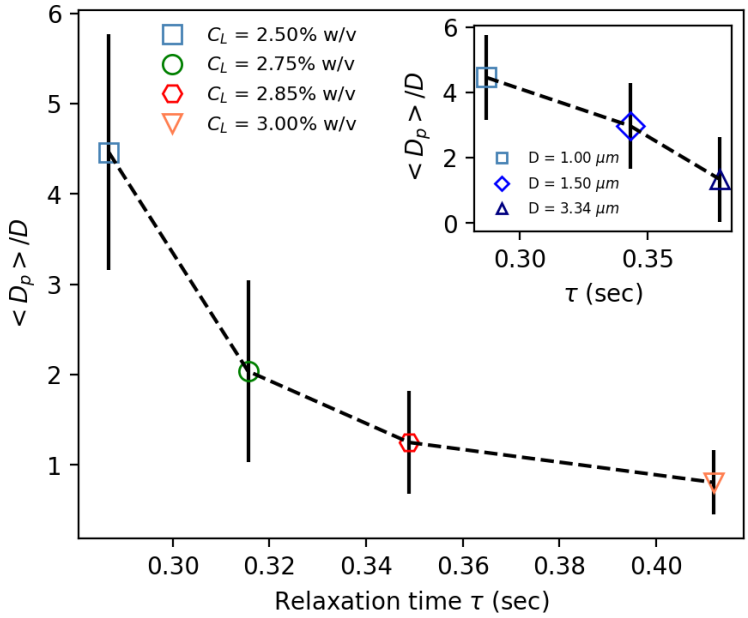

Supplementary Fig. S14: Pore size ratio $< D_p > /D$, the ratio of average pore diameter $< D_p >$ and the diameter of the trapped particle (D=1 μm), is plotted vs. characteristic relaxation time τ.

References

[1] Jan Gieseler, Juan Ruben Gomez-Solano, Alessandro Magazzù, Isaac Pérez Castillo, Laura Pérez García, Marta Gironella-Torrent, Xavier Viader-Godoy, Felix Ritort, Giuseppe Pesce, Alejandro V. Arzola, Karen Volke-Sepúlveda, and Giovanni Volpe. Optical tweezers — from calibration to applications: a tutorial. *Adv. Opt. Photon.*, 13(1):74–241, Mar 2021.